Journal of Applied Physics

RESEARCH ARTICLE | JUNE 17 2025

A reflective broadband metasurface-based cross-polarization converter (CPC) for Ku and K bands

Mahdi Salimitorkamani ; Elham Baladi ; Mehdi Mehranpour ; Hayrettin Odabasi

J. Appl. Phys. 137, 233104 (2025)
https://doi.org/10.1063/5.0251865

AIP Publishing

Journal of Applied Physics ARTICLE pubs.aip.org/aip/jap

A reflective broadband metasurface-based cross-polarization converter (CPC) for Ku and K bands

Cite as: J. Appl. Phys. **137**, 233104 (2025); doi: 10.1063/5.0251865
Submitted: 5 December 2024 · Accepted: 1 June 2025 ·
Published Online: 17 June 2025

Mahdi Salimitorkamani,[1,a)] Elham Baladi,[2] Mehdi Mehranpour,[3] and Hayrettin Odabasi[1]

AFFILIATIONS

[1]Department of Electrical and Electronics Engineering, Eskisehir Osmangazi University, Eskisehir, Turkey
[2]Department of Electrical and Computer Engineering, Polytechnique Montreal, Montreal, Quebec QC H3T 1J4, Canada
[3]Department of Electrical and Computer Engineering, University of Mohaghegh Ardabili (UMA), Ardabil, Iran

[a)]**Author to whom correspondence should be addressed:** mehdi.s6453@gmail.com

ABSTRACT

This study presents a broadband cross-polarization conversion metasurface (CPCM) designed for operation in the Ku and K bands. The CPCM unit cell consists of an octagonal ring with two diagonal parasitic arms, which extend within the ring and are thickened with a curvature on the top surface of a substrate, backed by a copper layer. The metasurface efficiently converts a linearly polarized incident electromagnetic (EM) wave into its cross-polarized counterpart over an ultra-wideband frequency range of 13.4–33.6 GHz. The polarization conversion ratio of the proposed structure exceeds 87% at the operating frequencies for normally incident waves and remains above 80% in a Ku band for angles up to 30° for both TE (transverse electric) and TM (transverse magnetic) polarized EM waves. The surface current distribution was thoroughly examined to explain the high-efficiency and ultra-broadband cross-polarization conversion. A good agreement was observed between measured and simulation results, indicating the promising potential of this structure in applications, such as polarization-controlled devices, stealth surfaces, and antennas.

I. INTRODUCTION

Polarization, defined as the orientation of the oscillating electric (E) field in an electromagnetic (EM) waves, is a crucial parameter for various applications. It is broadly classified into three types: linear, circular, and elliptical.[1] Controlling the polarization of EM waves is vital for ensuring optimal functionality for numerous applications, including communications, navigation, and radar systems.[1–4] For instance, in communications, a polarization mismatch can significantly reduce the performance and efficiency of a communication channel. This mismatch can be mitigated by employing different polarizations, such as circular or orthogonal polarizations.[2] Despite the advantages of circular polarization, linear polarization is more widely utilized in wireless communication applications.[2] Furthermore, using orthogonal polarizations can substantially increase the channel capacity of a communication system.[5] Conventionally, polarization control was achieved based on Faraday's effect and optical activity in natural materials.[6,7] However, these methods often exhibit limitations, such as increased thickness, limited bandwidth, restricted angular performance of incident waves, and added design complexity.[7] To address these challenges, metasurface-based polarization converters have been extensively studied over the past decade.[8]

Metasurfaces (MTSs), planar periodic structures composed of subwavelength unit cells, exhibit extraordinary EM properties not found in nature and can be utilized to control various characteristics of EM waves.[9] MTSs offer significant advantages for polarization control due to their low profile, lightweight, and broad bandwidth.[8] Various anisotropic MTS structures for polarization conversion have been studied in the literature, operating across different EM frequency bands[10–13] with various functionalities, such as cross-polarization and linear to circular polarization conversion. Typically, polarization converters based on MTSs are categorized into three groups: transmissive types,[14–17] reflective types,[18–21] and hybrid types.[22–24] Transmissive types generally involve a multi-layer

structure, making their manufacturing processes more complex than those of the reflective types.[20] Depending on the intended applications, the polarization converter can be designed to function either as a cross-polarization converter[25–30] or as a linear to circular polarization converter (LP to CP).[31,32] For example, in,[33] a polarization conversion ratio (PCR) exceeding 90% was demonstrated over a wide frequency range, but the design required a multi-layer structure, limiting its compactness and ease of fabrication. Similarly, ultra-wideband converters with high PCR have been reported in Refs. 34 and 35, but these designs either require multilayer substrates or vias, complicating the fabrication process. Recent designs with improved angular stability and bandwidth, such as Ref. 19, rely on costly and structurally soft materials, such as PTFE, which are challenging to process and less durable.[36] Thus, despite significant advancements, the development of broadband, compact, angularly stable, and cost-effective polarization converters remains a challenge.[20,37] A single-layer, compact, cost-effective, structurally simplified, and efficient design without the need for vias is beneficial for cross-polarization conversion (CPC) applications.

In this work, we present a compact, ultra-broadband, and high-efficiency cross-polarization conversion metasurface (CPCM) with angular stability. The proposed design effectively transforms incident electromagnetic waves into their orthogonal counterparts over the Ku and K bands (13.4–33.6 GHz), achieving a PCR greater than 87% within this range. Furthermore, the average PCR remains above 80% for incidence angles up to 30° and frequencies up to 26 GHz. The proposed design achieves an optimal balance between bandwidth, efficiency, compactness, angular stability, and cost-effectiveness, making it an ideal candidate for practical applications.

II. ANALYSIS AND DISCUSSION

A. Unit cell design

Figures 1(a) and 1(b) illustrate the configuration of the proposed unit cell for the cross-polarization converter. The unit cell is designed on a Rogers RO4003 substrate with a dielectric constant of 3.55 and a loss tangent (tan δ) of 0.0027. The substrate has a thickness of 1.52 mm and is backed by a copper layer with a conductivity of $\sigma = 5.80 \times 10^7$ S/m. The unit cell consists of an octagonal ring element combined with two oblique lines. Additionally, the octagonal ring is internally connected to the oblique lines through gradual curved lines. All design parameters are detailed in the caption of Fig. 1. The proposed unit cell was simulated, optimized, and analyzed using CST Microwave Studio.[38] The frequency domain solver was employed with periodic boundary conditions in the x and y directions, while open boundaries were applied in the z direction.

B. Theoretical analysis

A subwavelength MTS unit cell generally exhibits both electric and magnetic dipole effects, which can be characterized by its electromagnetic polarizabilities.[39] The electric and magnetic polarizabilities of the elements describe the relationship between their dipole moments and the corresponding local average electric and magnetic fields. These dipole moments can be expressed in terms of the local fields as

$$\begin{bmatrix} p \\ m \end{bmatrix} = \begin{bmatrix} p_{ee} & p_{em} \\ p_{me} & p_{mm} \end{bmatrix} \begin{bmatrix} E \\ H \end{bmatrix}, \tag{1}$$

where $p = \begin{bmatrix} p_x & p_y \end{bmatrix}$ and $m = \begin{bmatrix} m_x & m_y \end{bmatrix}$ denote the electric and magnetic dipole moments, respectively, and E and H are the local electric and magnetic fields. The impedance of the metasurface is influenced by its electric and magnetic responses and can be represented as $\eta(\omega) = \sqrt{\frac{\mu(\omega)}{\epsilon(\omega)}}$, where $\mu(\omega)$ and $\epsilon(\omega)$ are the frequency-dependent magnetic permeability and electric permittivity, respectively. The reflection coefficient under normal incidence, $R(\omega)$, is given by

$$R(\omega) = \frac{\eta(\omega) - \eta_0}{\eta(\omega) + \eta_0}, \tag{2}$$

where $\eta_0 = 377\,\Omega$. The reflection coefficient $R(\omega)$ is frequency-dependent and can be expressed as a complex quantity, $|R(\omega)|e^{i\varphi(\omega)}$, where $\varphi(\omega)$ is the phase of the reflected wave. From Eq. (2), it

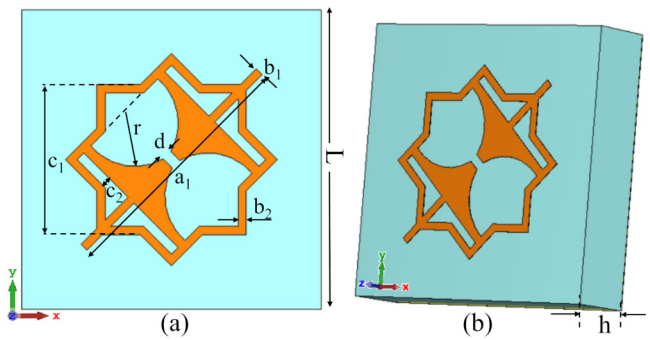

FIG. 1. (a) Front view and (b) a 3D view of the proposed polarization converter unit cell. Design parameters (all in mm) are given as $L = 5.8$, $a_1 = 4.8$, $b_1 = b_2 = 0.16$, $c_1 = 2.9$, $c_2 = 0.18$, $r = 1.12$, and $d = 0.2$.

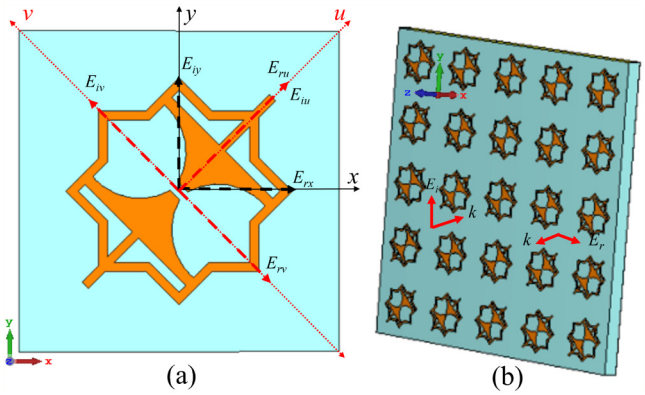

FIG. 2. (a) The proposed unit cell with the x–y axes and the orthogonal axes u and v. (b) Schematic of the proposed CPCM when exposed to illumination by a y-polarized EM wave.

follows that when the impedance of the MTS greatly exceeds that of free space, the magnitude of the reflection coefficient approaches unity, and its phase becomes zero degrees (0°). This indicates that the MTS acts as a high-impedance surface (HIS) or an artificial magnetic conductor (AMC), effectively reflecting electromagnetic waves with unity magnitude and zero phase across the frequency spectrum.

Due to symmetry along the diagonal direction of the unit cell, the performance under x-polarized incidence mirrors that under y-polarized incidence. Consequently, the study focuses on x-polarized incidence. To analyze the polarization conversion mechanism, the u- and v-axes are introduced by rotating the x and y axes counterclockwise by 45°, as shown in Fig. 2(a). For an x-polarized incident wave, $\vec{E}xi = \vec{E}xi\vec{e_x}$, while for a y-polarized wave, $\vec{E}yi = \vec{E}yi\vec{e_y}$, where $\vec{e_x}$ and $\vec{e_y}$ are unit vectors along the x and y axes, respectively.[40] A y-polarized wave incident on the MTS can be decomposed along the u- and v-axes as $\vec{E}yi = \vec{E}ui + \vec{E}vi$, with the reflected field $\vec{E}yr = \vec{E}ur + \vec{E}vr$. Therefore, the reflected EM wave along the u and v directions can be written as[41]

$$\vec{E}_{yr} = \vec{u}\,r_{uu}\left|\vec{E}_{ui}\right|e^{j(kz+\varphi_{uu})} + \vec{v}\,r_{vv}\left|\vec{E}_{vi}\right|e^{j(kz+\varphi_{vv})}. \quad (3)$$

Polarization conversion occurs when the electric field component in the +u direction is reflected with the same amplitude and direction, whereas the v component is reflected in the opposite direction but with an equal magnitude, resulting in a cross-polarized field. For this to occur, it is required that $|r_{uu}| = |r_{vv}| = 1$ and $\Delta\varphi_{uv} = 2k\pi \pm 180°$ (where k is an integer).[20,42] Figure 2(b) illustrates the proposed CPCM illuminated by a y-polarized wave, which is reflected as an x-polarized wave. The reflection coefficient comprises two components: a co-polarized coefficient, r_{xx} (or r_{yy}), retaining the same polarization as the incident wave, and a cross-polarized coefficient, r_{yx} (or r_{xy}), indicating a reflected field component orthogonal to the incident field.[40] The PCR for an x-polarized incident wave is calculated as

$$PCR = \frac{\left|r_{yx}^2\right|}{\left|r_{yx}^2\right| + \left|r_{xx}^2\right|}. \quad (4)$$

An additional parameter of interest is the azimuthal angle α, which quantifies the angle between the field components and provides further insight into the behavior of the CPCM. It is computed as[43]

$$\alpha = \arctan\left(r_{yx}/r_{xx}\right). \quad (5)$$

C. Simulation results

Figures 3(a)–3(d) depict the design process and the evolution of the proposed CPCM unit cell along with the respective reflection

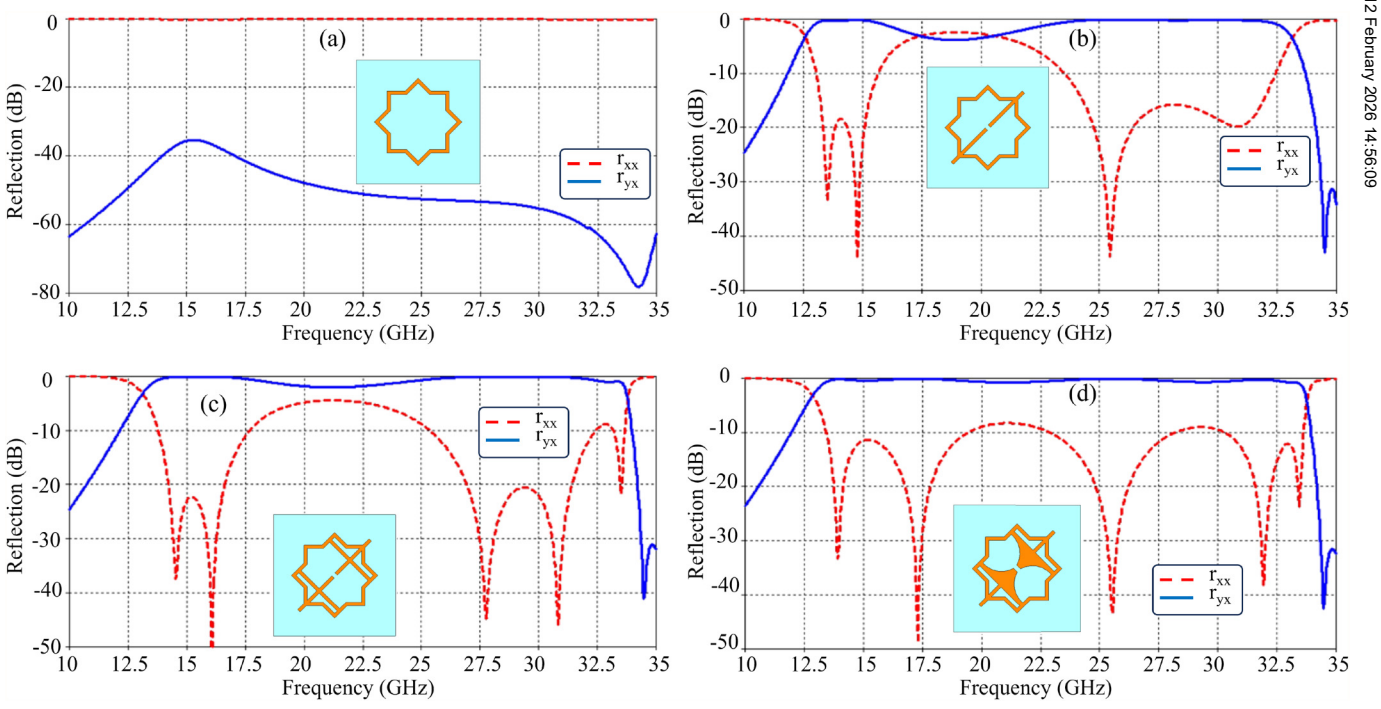

FIG. 3. The evolution of the unit cell and the corresponding reflection properties of the proposed reflective anisotropic MTS with (a) an octagonal ring, (b) an octagonal ring along two parasitic arms at 45° with respect to the x–y axes, (c) an octagonal ring with two stretched parasitic arms toward the center, and (d) the final proposed structure.

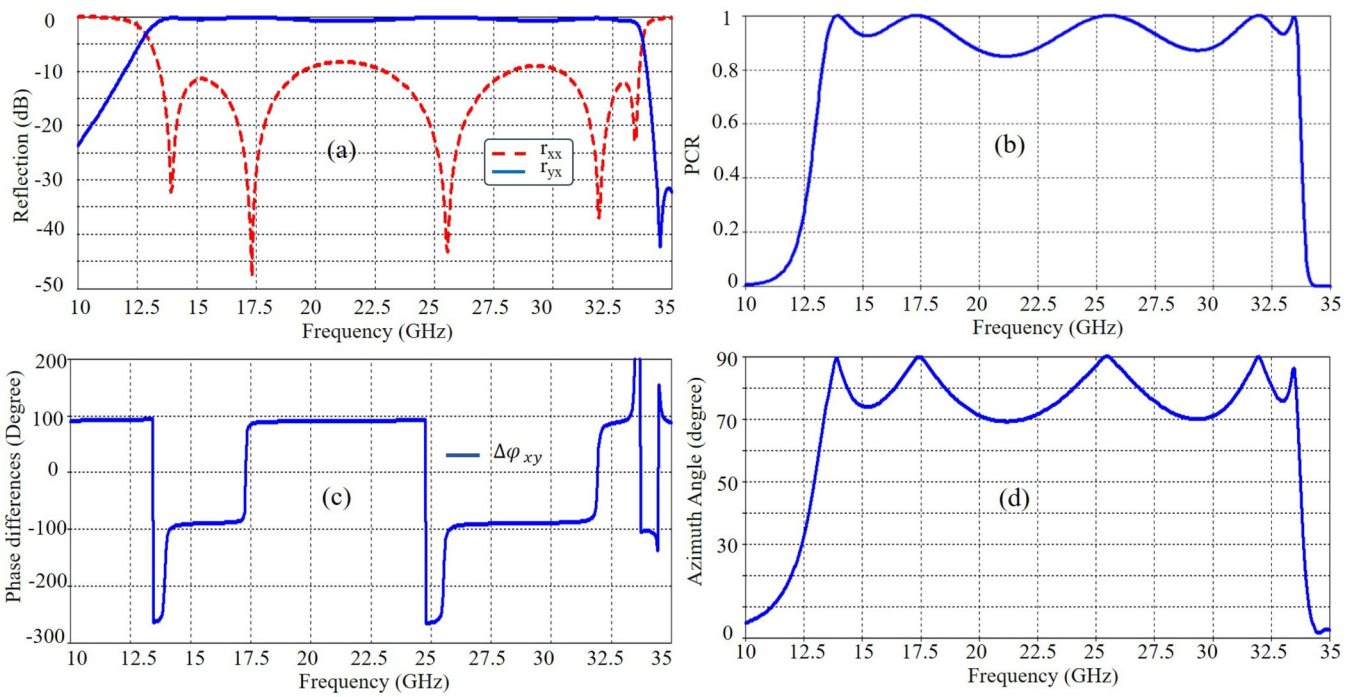

FIG. 4. Simulation results for (a) the reflection coefficient (r_{xx} and r_{yx}) of the proposed design, (b) the polarization conversion ratio (PCR), (c) the phase difference ($\Delta\phi_{xy}$) between r_{xx} and r_{yx}, and (d) the polarization azimuth angle.

characteristics for each geometry. Figure 3(a) illustrates an octagonal ring where the parameter r_{xx} is nearly equal to 0 dB, while r_{yx} is below −50 dB on average, indicating that no polarization conversion occurs in this state. By adding two diagonal parasitic arms to the ring as depicted in Fig. 3(b), the cross-polarization (r_{yx}) increases significantly within the frequency range of interest (13.4–33.6 GHz). Nonetheless, the cross-polarization is still low between 15.5 and 24 GHz. To improve the polarization conversion in this region, the

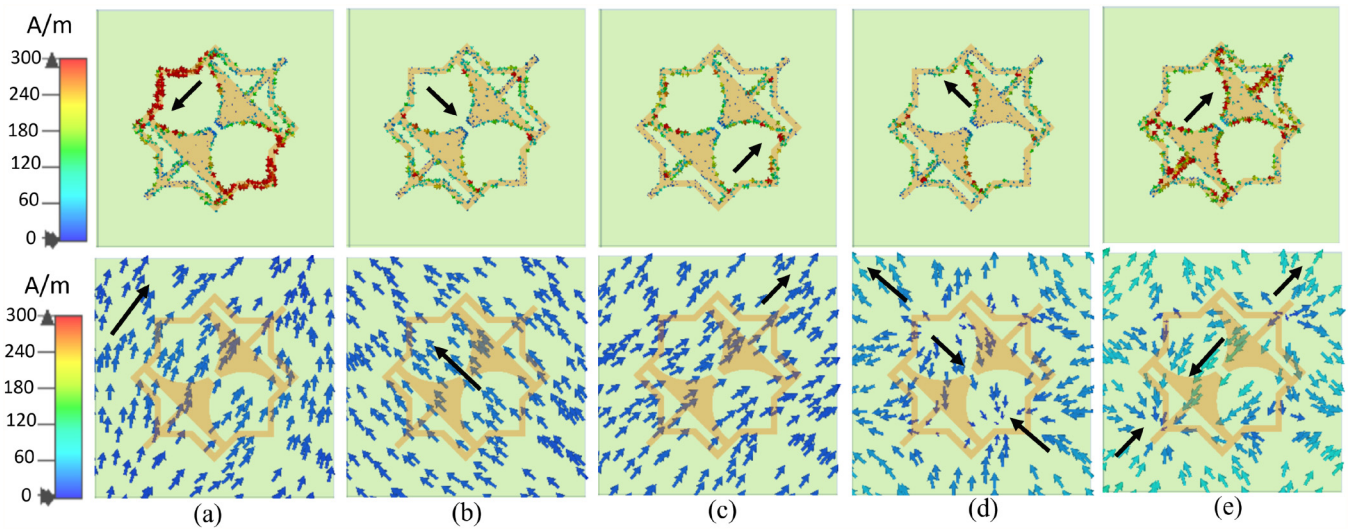

FIG. 5. Distribution of surface currents on the top and bottom metallic layers of the proposed anisotropic reflective unit cell at different resonance frequencies: (a) 13.3, (b) 17.3, (c) 25.7, (d) 32.2, and (e) 33.1 GHz.

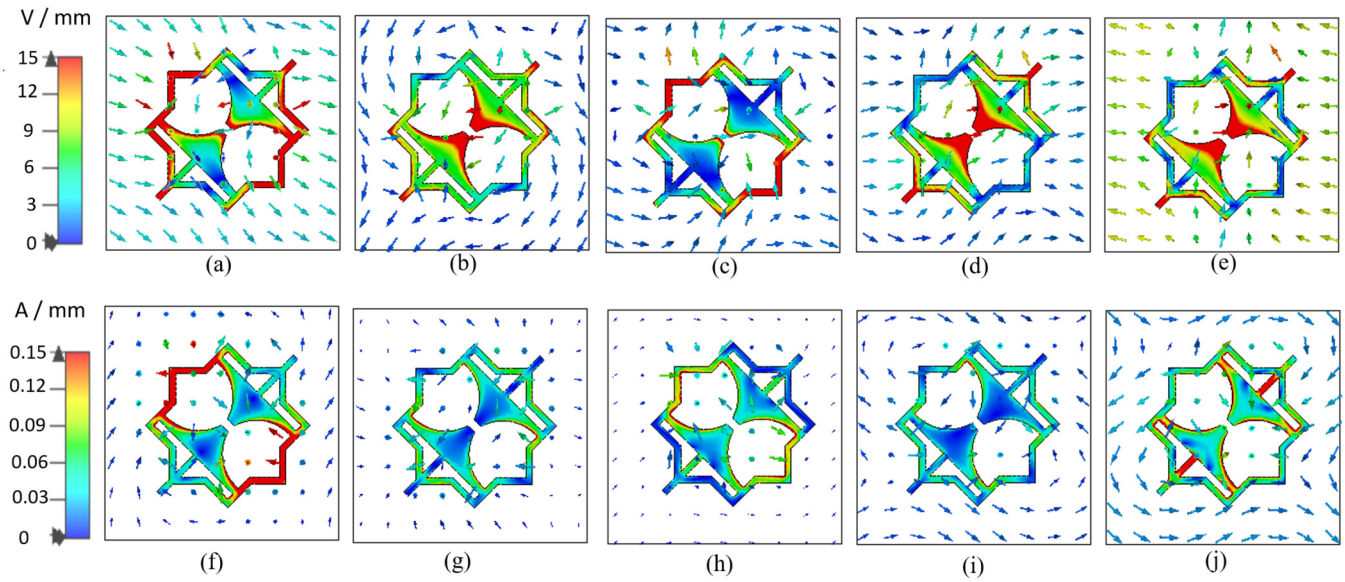

FIG. 6. The electric and magnetic field intensities at different resonance frequencies: E-field intensity at (a) 13.3, (b) 17.3, (c) 25.7, (d) 32.2, and (e) 33.1 GHz; H-field intensity at (f) 13.3, (g) 17.3, (h) 25.7, (i) 32.2, and (j) 33.1 GHz.

diagonal parasitic arms are extended within the octagonal ring and thickened with a curvature as shown in Figs. 3(c) and 3(d), respectively. As can be seen from Fig. 3(d), the proposed structure achieves a broadband polarization conversion between 13.4 and 33.4 GHz.

The efficiency of the polarization converter is evaluated using the PCR parameter and the azimuth angle (α). A PCR approaching 1 and the azimuth angle close to 90° indicates nearly 100% polarization conversion efficiency. Figures 4(a) and 4(b) show the reflection coefficients (r_{xx} and r_{yx}) of the proposed unit cell structure of the proposed unit cell structure and the corresponding polarization conversion ratio (PCR), respectively. The simulated PCR exceeds 87% across the frequency range of interest, indicating an efficient polarization conversion. Figure 4(c) illustrates the phase difference between r_{xx} and r_{yx} ($\Delta\phi_{xy}$ = arg (r_{xx}) - arg (r_{yx})), which remains stable near $\pm(2n+1)90^\circ$ within the polarization conversion bands an essential condition for achieving linear-to-linear polarization rotation. The azimuth angle, presented in Fig. 4(d), exceeds 70° throughout the Ku and K bands, with complete 90° polarization rotation observed at 13.88, 17.53, 25.58, and 31.96 GHz. These results confirm the proposed structure's high efficiency in cross-polarization conversion.

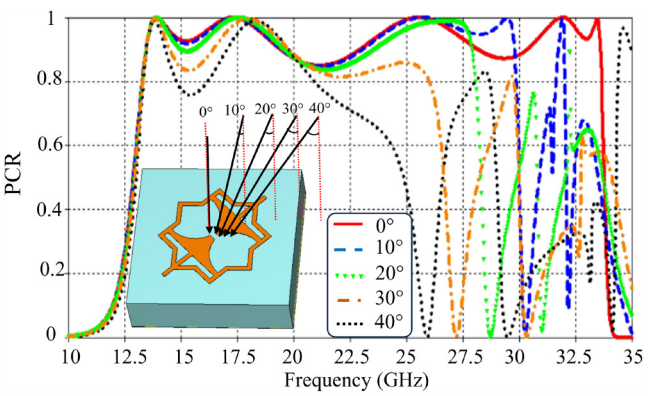

FIG. 7. Response of the proposed reflective unit cell under various oblique incident angles.

D. Surface current analysis

To gain a deeper understanding of the broad-range polarization conversion mechanism of the proposed unit cell, we analyze the distribution of surface currents on both the top and ground planes. This surface current analysis is performed at five discrete resonance frequencies: 13.3, 17.3, 25.7, 32.2, and 33.1 GHz, as shown in Fig. 5, labeled (a)–(e). Magnetic (plasmonic) resonances occur when the currents flow in opposite directions on the top and bottom metallic layers, while electric or composite EM resonances are induced in other cases.[19,27] At 13.3 and 17.3 GHz [Figs. 5(a) and 5(b)], the currents on the top layer of the MTS unit cell flow opposite to those on the ground plane, resulting in magnetic resonances. At 25.7 GHz [Fig. 5(c)], an electric resonance is induced as the currents align between the top and ground planes. At 32.2 and 33.1 GHz [Figs. 5(d) and 5(e)], both magnetic and electric resonances are simultaneously excited, leading to a composite EM resonance. The ultra-broadband performance is attributed to the occurrence of multiple resonances across the frequency range,

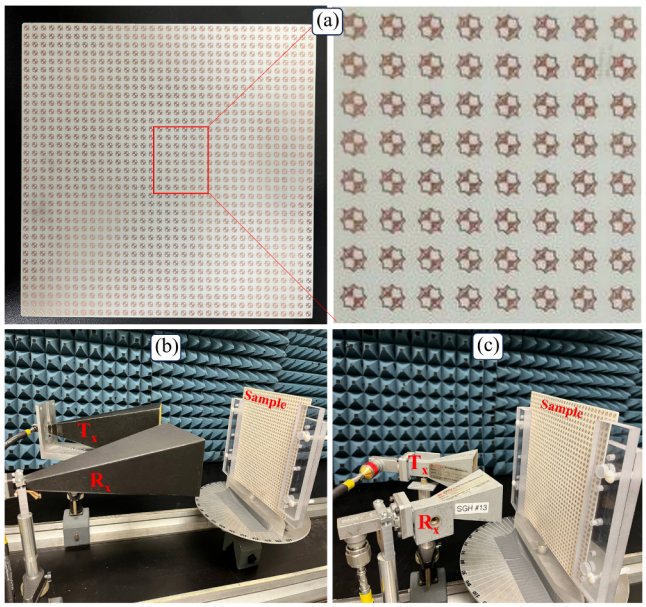

FIG. 8. (a) Fabricated sample, (b) a measurement setup using horn antennas covering the frequency range of 12.4–18.5 GHz, and (c) a measurement setup for frequencies in the range of 18.4–26.5 GHz.

which are essential for achieving both high-efficiency and ultra-broadband cross-polarization conversion.

Figure 6 illustrates the electric (top row) and magnetic (bottom row) field intensity distributions at the resonance frequencies for the proposed CPCM unit cell. Each column corresponds to a specific resonant mode of interest. In the electric field plots [Figs. 6(a)–6(e)], strong field localization can be observed around the edges and gaps of the gradual curved lines. The red regions

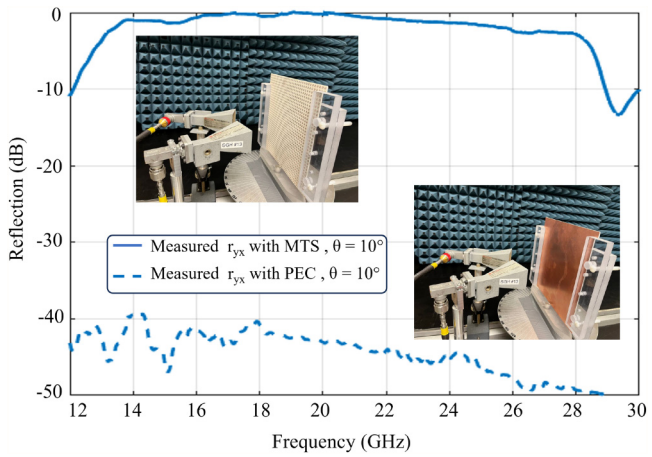

FIG. 10. Comparison of the measured r_{yx} between a PEC reflector and the fabricated MTS sample.

indicate areas of maximum electric field enhancement, corresponding to capacitive hot spots where polarization conversion is most active. The asymmetry in the field distribution supports the presence of strong anisotropic coupling, which is essential for achieving high-efficiency linear cross-polarization conversion. The magnetic field intensity plots [Figs. 6(f)–6(j)] demonstrate complementary behavior, with enhanced H-field intensities concentrated in regions where current loops or circulating displacement currents form. These circulating fields confirm the excitation of magnetic resonant modes, which work together with the electric resonances to support bi-anisotropic behavior necessary for polarization rotation. Moreover, as shown in Fig. 6, the field is directed either upward or downward relative to the ground plane. Together, the E-field and H-field distributions confirm the presence of hybrid electric-

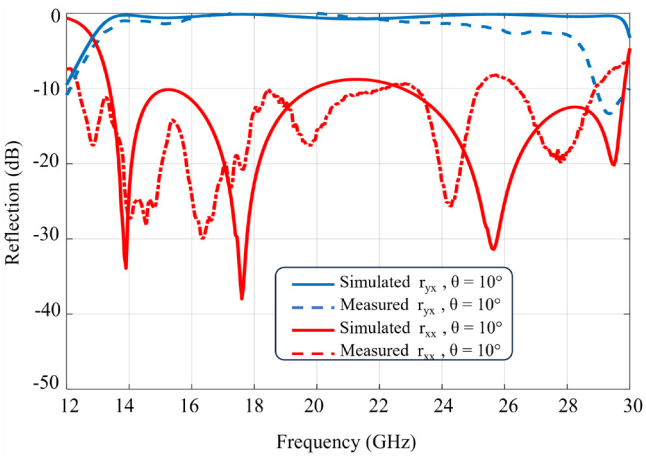

FIG. 9. Comparison of the simulated r_{xx} and r_{yx} with the measured counterparts when $\theta = 10°$.

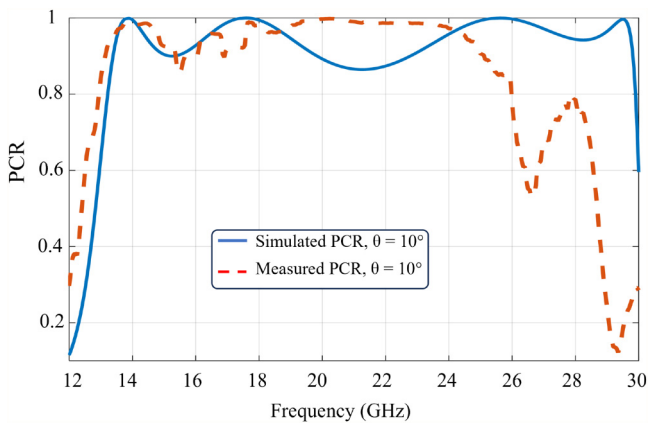

FIG. 11. Comparison of the simulated and measured PCR values over frequency.

TABLE I. Performance comparison of the proposed polarization converter with other recently published single-layer linear polarization converters.

Reference	Frequency range (GHz)	Unit cell size (with respect to λ_{max})	Percentile bandwidth (%)	Substrate	Angular stability	PCR (%)
7	8–18.5	$0.13\lambda \times 0.13\lambda \times 0.064\lambda$	80	FR4	45	90
19	9.83–29.37	$0.2\lambda \times 0.2\lambda \times 0.083\lambda$	99.69	PTFE	40	90
21	13–26	$0.3\lambda \times 0.3\lambda \times 0.069\lambda$	66	FR4	40	90
27	11.5–21.8	$0.3\lambda \times 0.3\lambda \times 0.076\lambda$	19.4, 37.5	FR4	40	96
29	8.52–17.93	$0.2\lambda \times 0.2\lambda \times 0.068\lambda$	71	RO4003	45	90
30	9.04–20.83	$0.21\lambda \times 0.21\lambda \times 0.066\lambda$	79	F4B-2	30	90
45	6.67–17.1	$0.26\lambda \times 0.26\lambda \times 0.077\lambda$	87.7	F4B-2	n/a	90
46	6.1–16.5	$0.14\lambda \times 0.14\lambda \times 0.06\lambda$	92	FR4	45	78
This work	13.4–33.5	$0.25\lambda \times 0.25\lambda \times 0.069\lambda$	86	RO4003	40	87

magnetic modes and validate the physical origin of the observed resonance peaks and polarization conversion in the S-parameter results.

E. Angular stability

Another important parameter in CPC structures is angular stability. Although polarization conversion can be achieved through anisotropic structures in a reflection mode, these structures are sensitive to the angle of incidence, and their response often varies with oblique incidence. To evaluate angular stability, the incident angle (θ) is varied from 0° to 40°, and the results are shown in Fig. 7. As the incident angle increases, the bandwidth gradually decreases, as indicated by the PCR parameter in Fig. 7. This reduction in bandwidth at higher frequencies is mainly due to the longer electrical path at higher incidence angles.[44] This effect is less pronounced at lower frequencies, where the metasurface unit cells are electrically smaller, making them more stable with respect to the angle of incidence.

III. EXPERIMENTAL RESULTS

To validate the simulation results, a prototype consisting of 35×35 unit cells was fabricated on a RO4003 substrate, with overall dimensions of $203 \times 203 \times 1.52\ \text{mm}^3$. Figure 8 presents the fabricated metasurface (MTS) prototype alongside the experimental setup. Two linearly polarized standard horn antennas, operating in the frequency ranges of 12.4–18.5 GHz [Fig. 8(b)] and 18.4–26.5 GHz [Fig. 8(c)], were used to transmit the incident EM wave and capture the reflected wave from the structure. Due to limitations in the available horn antenna pairs, measurements were conducted only within these frequency ranges, covering the majority of the operational band except for the portion from 26.5 to 33.6 GHz. To demonstrate the effectiveness of the proposed structure in converting incident linearly polarized EM waves to cross-polarized components, the experimental setup positioned the transmitting horn antenna for co-polarization, while the receiving horn antenna was oriented to capture the cross-polarized reflected waves. An incidence angle of 10° was employed to minimize interference between the transmitted and received signals and to prevent any potential blockage. The fabricated sample was vertically mounted in front of the horn antennas during the measurements, as shown in Figs. 8(b) and 8(c). A Keysight N5224B Vector Network Analyzer (VNA) was used for measurements. The reflection coefficients r_{xx} and r_{yx} of the proposed structure were measured in an anechoic chamber and compared with simulation results for an incidence angle $\theta = 10°$, as shown in Fig. 9. The measurements show strong agreement with the simulation results. Figure 10 compares the cross-polarized reflection coefficient r_{yx} for the fabricated metasurface and a PEC reference panel. The results demonstrate that the r_{yx} for the fabricated MTS is, on average, 40 dB higher than that of the PEC, confirming the efficient conversion of the incident polarization to its cross-polarized counterpart. Finally, Fig. 11 compares the PCR values obtained from simulations and measurements. The results confirm high polarization conversion efficiency within the measured frequency range, despite the limited size of the fabricated prototype compared to the infinite periodic boundary conditions used in simulations. A detailed comparison with previously published works is provided in Table I.

IV. CONCLUDING REMARKS

In this work, a broadband metasurface-based cross-polarization converter designed for operation in the Ku and K bands is presented. The metasurface unit cell features an octagonal ring combined with 45° rotated anisotropic oblique lines, enabling efficient polarization conversion of linearly polarized incident electromagnetic waves into their corresponding cross-polarized components. The proposed design achieves an ultra-wideband performance across the 13.4–33.6 GHz frequency range, encompassing both the Ku and K bands. The polarization conversion ratio (PCR) exceeds 87% for normally incident waves within the operational frequency band, while maintaining an azimuth angle greater than 70°. Additionally, the structure demonstrates good angular stability, achieving a PCR greater than 80% between 13.4 and 26 GHz for incidence angles up to 30°. Surface current analyses provide valuable insights into the underlying operational mechanisms, revealing the contributions of electric, magnetic, and composite electromagnetic resonances to the broadband performance. Strong agreement between simulated and measured results is obtained. The proposed design has a potential use for a range of applications requiring efficient and broadband polarization control in the Ku and K bands.

AUTHOR DECLARATIONS

Conflict of Interest

The authors have no conflicts to disclose.

Author Contributions

Mahdi Salimitorkamani: Conceptualization (lead); Formal analysis (lead); Investigation (lead); Methodology (lead); Software (lead); Writing – original draft (lead). **Elham Baladi:** Supervision (supporting); Validation (lead); Writing – review & editing (equal). **Mehdi Mehranpour:** Formal analysis (supporting); Investigation (supporting). **Hayrettin Odabasi:** Investigation (equal); Supervision (equal); Writing – review & editing (equal).

DATA AVAILABILITY

Data sharing is not applicable to this article as no new data were created or analyzed in this study.

REFERENCES

[1]M. Beruete, M. Navarro-Cía, M. Sorolla, and I. Campillo, "Polarization selection with stacked hole array metamaterial," J. Appl. Phys. **103**, 053102 (2008).
[2]C. Guo, F. Liu, S. Chen, C. Feng, and Z. Zeng, "Advances on exploiting polarization in wireless communications: Channels, technologies, and applications," IEEE Commun. Surv. Tutor. **19**, 125–166 (2016).
[3]H.-R. Chuang and L.-C. Kuo, "3D FDTD design analysis of a 2.4 GHz polarization-diversity printed dipole antenna with integrated balun and polarization-switching circuit for WLAN and wireless communication applications," IEEE Trans. Microwave Theory Tech. **51**, 374–381 (2003).
[4]M. R. Andrews, P. P. Mitra, and R. DeCarvalho, "Tripling the capacity of wireless communications using electromagnetic polarization," Nature **409**, 316–318 (2001).
[5]T. Svantesson, M. A. Jensen, and J. W. Wallace, "Analysis of electromagnetic field polarizations in multiantenna systems," IEEE Trans. Wirel. Commun. **3**, 641–646 (2004).
[6]Y. Ye and S. He, "90° polarization rotator using a bilayered chiral metamaterial with giant optical activity," Appl. Phys. Lett. **96**, 203501 (2010).
[7]A. Rashid, M. Murtaza, S. A. A. Zaidi, H. Zaki, and F. A. Tahir, "A single-layer, wideband and angularly stable metasurface based polarization converter for linear-to-linear cross-polarization conversion," PLoS One **18**, e0280469 (2023).
[8]N. Pouyanfar, J. Nourinia, and C. Ghobadi, "Multiband and multifunctional polarization converter using an asymmetric metasurface," Sci. Rep. **11**, 9306 (2021).
[9]C. L. Holloway, E. F. Kuester, J. A. Gordon, J. O'Hara, J. Booth, and D. R. Smith, "An overview of the theory and applications of metasurfaces: The two-dimensional equivalents of metamaterials," IEEE Antennas Propag. Mag. **54**, 10–35 (2012).
[10]Q. Zheng, C. Guo, G. A. Vandenbosch, P. Yuan, and J. Ding, "Ultra-broadband and high-efficiency reflective polarization rotator based on fractal metasurface with multiple plasmon resonances," Opt. Commun. **449**, 73–78 (2019).
[11]F. Li, H. Chen, L. Zhang, Y. Zhou, J. Xie, L. Deng, and V. G. Harris, "Compact high-efficiency broadband metamaterial polarizing reflector at microwave frequencies," IEEE Trans. Microwave Theory Tech. **67**, 606–614 (2018).
[12]H. Sun, C. Gu, X. Chen, Z. Li, L. Liu, and F. Martín, "Ultra-wideband and broad-angle linear polarization conversion metasurface," J. Appl. Phys. **121**, 174902 (2017).
[13]B. Khan, S. Ullah, B. Kamal *et al.*, "Design and analysis of a wide band cross-polarization converting metasurface," in *2019 International Conference on Communication Technologies (ComTech)* (IEEE, 2019), pp. 9–12.
[14]Z. Cui, Z. Xiao, M. Chen, F. Lv, and Q. Xu, "A transmissive linear polarization and circular polarization cross polarization converter based on all-dielectric metasurface," J. Electron. Mater. **50**, 4207–4214 (2021).
[15]D.-J. Liu, Z.-Y. Xiao, X.-L. Ma, and Z.-H. Wang, "Broadband asymmetric transmission and multi-band 90° polarization rotator of linearly polarized wave based on multi-layered metamaterial," Opt. Commun. **354**, 272–276 (2015).
[16]Q. Zeng, W. Ren, H. Zhao, Z. Xue, and W. Li, "Dual-band transmission-type circular polariser based on frequency selective surfaces," IET Microw. Antennas Propag. **13**, 216–222 (2019).
[17]X. Huang, X. Ma, H. Gao, L. Guo, and X. Li, "Ultra-wideband linear-polarization conversion metasurface with high-efficient asymmetric transmission," Appl. Phys. A **129**, 278 (2023).
[18]Abdullah, B. Kamal, S. Ullah, B. Khan, H. Ali, and T. Rahim, "Cross polarization conversion metasurface for fixed wireless and Ku-band applications," Int. J. Commun. Syst. **35**, e5033 (2022).
[19]B. Zhang, C. Zhu, R. Zhang, X. Yang, Y. Wang, and X. Liu, "Ultra-broadband angular-stable reflective linear to cross polarization converter," Electronics **11**, 3487 (2022).
[20]F. Tutar and G. Ozturk, "An effective metasurface-based linear and circular polarization converter for C- and X-band applications," Opt. Mater. **128**, 112355 (2022).
[21]T. Ahmad, A. A. Rahim, R. M. H. Bilal, A. Noor, H. Maab, M. A. Naveed, A. Madni, M. M. Ali, and M. A. Saeed, "Ultrawideband cross-polarization converter using anisotropic reflective metasurface," Electronics **11**, 487 (2022).
[22]Z. Tao, X. Wan, B. C. Pan, and T. J. Cui, "Reconfigurable conversions of reflection, transmission, and polarization states using active metasurface," Appl. Phys. Lett. **110**, 121901 (2017).
[23]H. Yang, S. C. Wang, P. Li, Y. He, and Y. J. Zhang, "A broadband multifunctional reconfigurable polarization conversion metasurface," IEEE Trans. Antennas Propag. **71**, 5759–5767 (2023).
[24]F. Ahmed, M. I. Khan, and F. A. Tahir, "A multifunctional polarization transforming metasurface for C-, X-, and K-band applications," IEEE Antennas Wirel. Propag. Lett. **20**, 2186–2190 (2021).
[25]M. I. Khan, Q. Fraz, and F. A. Tahir, "Ultra-wideband cross polarization conversion metasurface insensitive to incidence angle," J. Appl. Phys. **121**, 043105 (2017).
[26]I. Hossain, M. T. Islam, H. Alsaif, A. G. Alharbi, N. B. M. Sahar, and M. Samsuzzaman, "An angular stable triple-band anisotropic cross-polarization conversion metasurface," Results Phys. **37**, 105564 (2022).
[27]Z. Liu, B. Zhao, C. Jiao, L. Zhao, and X. Han, "Broadband cross-polarization conversion metasurface based on cross-shaped resonators," Appl. Phys. A **127**, 1–9 (2021).
[28]F. A. Tahir *et al.*, "A broadband metasurface for cross polarization conversion applications," in *2019 IEEE International Conference on Computational Electromagnetics (ICCEM)* (IEEE, 2019), pp. 1–2.
[29]B. Kamal, J. Chen, Y. Yin, J. Ren, and S. Ullah, "Wide band cross polarization converting metasurface based on circular split rings resonators," in *2020 IEEE International Conference on Computational Electromagnetics (ICCEM)* (IEEE, 2020), pp. 223–225.
[30]C. Liu, R. Gao, Q. Wang, and S. Liu, "A design of ultra-wideband linear cross-polarization conversion metasurface with high efficiency and ultra-thin thickness," J. Appl. Phys. **127**, 153103 (2020).
[31]M. I. Khan, Z. Khalid, and F. A. Tahir, "Linear and circular-polarization conversion in X-band using anisotropic metasurface," Sci. Rep. **9**, 4552 (2019).
[32]M. I. Khan, Y. Chen, B. Hu, N. Ullah, S. H. R. Bukhari, and S. Iqbal, "Multiband linear and circular polarization rotating metasurface based on multiple plasmonic resonances for C, X and K band applications," Sci. Rep. **10**, 17981 (2020).
[33]Y. Jia, Y. Liu, W. Zhang, and S. Gong, "Ultra-wideband and high-efficiency polarization rotator based on metasurface," Appl. Phys. Lett. **109**, 051901 (2016).
[34]R. Zaker and A. Sadeghzadeh, "A low-profile design of polarization rotation reflective surface for wideband RCS reduction," IEEE Antennas Wirel. Propag. Lett. **18**, 1794–1798 (2019).

[35]M. Xie, C. Chen, G. Xue, X. Fu, and J. Chen, "A ultra-wideband polarization conversion metasurfaces used for RCS reduction," in *2019 IEEE MTT-S International Microwave Biomedical Conference (IMBioC)* (IEEE, 2019), Vol. 1, pp. 1–3.
[36]"Rogers RO4003C laminate datasheet"; see https://www.rogerscorp.com/advanced-electronics-solutions/ro4000-series-laminates/ro4003c-laminates (last accessed November 15, 2024).
[37]H. Chen, J. Wang, H. Ma, S. Qu, Z. Xu, A. Zhang, M. Yan, and Y. Li, "Ultra-wideband polarization conversion metasurfaces based on multiple plasmon resonances," J. Appl. Phys. **115**, 154504 (2014).
[38]CST Studio Suite, "CST Microwave Studio version 2022; see https://www.3ds.com/products-services/simulia/products/cst-studio-suite/ (Dassault Systèmes, USA, 2022).
[39]V. S. Asadchy, A. Díaz-Rubio, and S. A. Tretyakov, "Bianisotropic metasurfaces: Physics and applications," Nanophotonics **7**, 1069–1094 (2018).
[40]Q. Zheng, C. Guo, G. A. Vandenbosch, P. Yuan, and J. Ding, "Dual-broadband highly efficient reflective multi-polarisation converter based on multi-order plasmon resonant metasurface," IET Microw. Antennas Propag. **14**, 967–972 (2020).
[41]M. Karamirad, C. Ghobadi, and J. Nourinia, "Metasurfaces for wideband and efficient polarization rotation," IEEE Trans. Antennas Propag. **69**, 1799–1804 (2020).
[42]M. A. Shukoor, S. Dey, S. K. Koul, A. K. Poddar, and U. L. Rohde, "Broadband linear-cross and circular-circular polarizers with minimal bandwidth reduction at higher oblique angles for RCS applications," Int. J. RF Microw. Comput.-Aided Eng. **31**, e22693 (2021).
[43]X. Huang, H. Yang, D. Zhang, and Y. Luo, "Ultrathin dual-band metasurface polarization converter," IEEE Trans. Antennas Propag. **67**, 4636–4641 (2019).
[44]X. Gao, X. Han, W.-P. Cao, H. O. Li, H. F. Ma, and T. J. Cui, "Ultrawideband and high-efficiency linear polarization converter based on double V-shaped metasurface," IEEE Trans. Antennas Propag. **63**, 3522–3530 (2015).
[45]J. Xu, R. Li, S. Wang, and T. Han, "Ultra-broadband linear polarization converter based on anisotropic metasurface," Opt. Express **26**, 26235–26241 (2018).
[46]A. Majeed and J. Zhang, "A study of linear-to-linear (LTL) cross-polarization conversion metasurface (CPCM) in microwave regime," Optik **274**, 170497 (2023).